

Non-linear Current-Voltage Dependence of the Superconducting Transition in 1-D Ultrananowire Al wires

Fabio Altomare,^{1, 2} Albert M. Chang,^{1, 2} Michael R. Melloch,³ Yuguang Hong,⁴ and Charles W. Tu⁴

¹*Physics Department, Duke University, Durham, NC 27707*

²*Physics Department, Purdue University, West Lafayette, IN 47906*

³*School of Electrical and Computer Engineering, Purdue University, West Lafayette, IN 47906*

⁴*Department of Computer and Electrical Engineering, UCSD, La Jolla, CA 92093*

(Dated: November 11, 2019)

The nonlinear current-voltage characteristics and linear resistance of two ultra-narrow aluminum wires with lateral dimensions below 10 nm have been studied as a function of temperature and magnetic field. Both wires ($\approx 10 \mu\text{m}$ and $100 \mu\text{m}$ long, resistance $\approx 8 \text{k}\Omega$ and $80 \text{k}\Omega$, respectively) exhibited superconducting tendency. While the superconducting transition near zero magnetic field follows closely the behavior expected from classical, thermally activated phase slips, by applying a field it evolves into a behavior more appropriately described by the non-classical, macroscopic quantum tunneling of phase slips.

PACS numbers: 74.78.Na, 74.25.Fy, 74.25.Ha, 74.40.+k

One-dimensional (1D) superconductivity has recently attracted much interest due to new techniques[1, 2, 3, 4, 5] which enable the fabrication of superconducting wires with lateral size smaller than the superconducting coherence length. In 1D superconductors, immediately below the transition, the phase of the order parameter becomes localized in one of many equivalent, meta-stable free energy minima within a tilted washboard landscape where the wave function of the complex order parameter can be represented by a helix of a fixed number of turns, which increases by one unit for each successive minimum. Fluctuations can cause the phase of the order parameter, in a spatially localized region of the wire, to move between adjacent minima thus changing the number of turns of the helix. During this process, the order parameter goes to zero, its phase changes by 2π and the region becomes normal thus producing a finite resistance. The mechanism responsible for the fluctuations dictates the shape of the normal-superconducting (N-S) transition. Langer and Ambegaokar[6], suggested Thermal Activation as the main mechanism for Phase Slip motion (TAPS) and this theory, extended by McCumber and Halperin[7] (LAMH from now on), predicts the following resistance and voltage drop across the superconductor:

$$R_{LAMH} = R_q \frac{\Omega}{k_B T} \exp\left(-\frac{\Delta F}{k_B T}\right) \quad (1)$$

$$V_{TAPS} = I_0 R_{LAMH} \sinh(I/I_0)$$

where $R_q = \pi\hbar/2e^2$, $\Omega = (L/\xi)(\Delta F/k_B T)^{1/2}(\hbar/\tau_{GL})$, $\Delta F = (8\sqrt{2}/3)(H_c^2/8\pi)A\xi$, $\tau_{GL} = (\pi/8)[\hbar/k_B(T - T_c)]$, $I_0 = 4ek_B T/h$, L is the wire length, T the temperature, k_B the Boltzmann constant, ΔF the free energy barrier between two consecutive minima, H_c the thermodynamical critical field, A the wire cross section, ξ the Ginzburg Landau (GL) superconducting coherence length, and τ_{GL} the GL relaxation time. While this theory has been successfully used[8] in explaining the N-S

transition in wide wires at $T \approx T_c$, disagreement with the experimental data appeared when Giordano[9] fabricated superconducting wires with diameters comparable to 10 nm. He suggested that, in thin wires, tunneling of the order parameter phase could be responsible for phase slippage (quantum tunnel of phase slips-QTPS) producing a resistance (GIO model from now on):

$$R_{GIO} = B_{GIO} R_q \frac{L}{\xi} \sqrt{\frac{\Delta F}{\hbar/\tau_{GL}}} \exp\left(-a_{GIO} \frac{\Delta F}{\hbar/\tau_{GL}}\right) \quad (2)$$

and, in analogy with the thermal case, we propose that the voltage should depend on the current as follows:

$$V_{QTPS} = I_{GIO} R_{GIO} \sinh(I/I_{GIO}) \quad (3)$$

where $I_{GIO} = 2e/(\pi\tau_{GL}a_{GIO})$, B_{GIO} and a_{GIO} are parameters of the order of unity. In this quantum case, a resistance similar to the Giordano expression (and numerically equivalent) has been recently derived, on a microscopic basis, by Golubev, Zaikin (GZ) et al.[10, 11]. In the quantum regime, both GZ and a more recent theory[12] predict a crossover from an exponential dependence to a power law behavior ($V \propto I^\nu$) in a limit where the energy dissipates via an effective 1-dimensional plasmon mode. Interestingly enough, the I-V characteristics we will present turn out to be well described by the power law model (and typical fits overlap the best fits obtained with the GIO model shown below). However from a theoretical point of view, it is not yet clear this regime is appropriate for our wire. In view of this uncertainty we will focus our discussion to the phenomenological approach discussed above and relegate additional analysis on the power law theory the EPAPS supplement[13]. To date, nearly all of the experimental work in this field [9, 14, 15] has focused on the shape of the N-S transition as a function of the temperature. Only recently, Rogachev et al.[16] have included the study of the non-linear current-voltage characteristics in constant current

	L μm	w nm	t nm	R_N kΩ	ρ $μΩcm$	l_e nm	$ξ$ nm	J_c $10^5 A/cm^2$
s1	10	6.9	9.0	8.3	5.1	7.6	94	12.1
s2	100	5.25	6.09	86	2.8	14.3	128	13.1

TABLE I: Parameters for sample s1 and s2. The parameters L (length), w (width), t (thickness), R_N (normal state resistance), ρ (resistivity), l_e (mean free path), ξ (GL coherence length), and J_c (critical current density), for the two samples s1 and s2. w, t, ρ and l_e have been deduced following the analysis in Altomare et al.[5] based on magnetoresistance measurements. ξ was calculated using $\xi = 0.85\sqrt{\xi_0}l_e$ where $\xi_0 = 1600$ nm is the GL superconducting coherence length.

mode (I-V from now on), in which V essentially exhibited an exponential dependence on I (Eq. 1). Extracting a linear resistance, they demonstrated that the transition in Nb and MoGe superconducting nanowires follows the LAMH theory over ≈ 11 orders of magnitude with minimal deviation. *Here in contrast, exploiting the non-linearity and including the quantum contribution in our analysis, it will be shown that QTPS contributions are crucial to obtaining an accurate description of the data.*

Our Al wires were fabricated by thermal evaporating the aluminum metal onto a narrow, 8 nm wide, MBE (molecular-beam-epitaxy) grown InP ridge. In the same step, the aluminum is also deposited on top of the four terminal Au/Ti measurement pads, ensuring good electrical contact without any insulating oxide layer in between (Fig. 1(a)-inset). Details of the fabrication, including the connections for a four-terminal measurement, have been described separately[5]. Magnetoresistance measurements[17] at 4.2 K (above T_c) were used to characterize the wires and to estimate the thickness of the surface oxide (≈ 3.5 nm on each exposed surface). Sample parameters, such as the effective wire width, thickness, mean free path and the GL coherence length, ξ , are summarized in Table 1. ξ , calculated from the dirty limit expression is ≈ 94 nm for the 10 μ m wire (s1) and ≈ 128 nm for the 100 μ m wire (s2), exceeding the lateral dimensions of 5-9 nm. For sample s2 the ratio ξ/w (>20) is much larger than what was obtained in previous work on 1D superconducting nanowires [1, 14, 15, 16].

The N-S transition of the nanowires, measured with a current of 1.6 nA, is presented in Fig. 1(a). It is possible to fit much of the zero magnetic field N-S transition data to the LAMH behavior, despite the presence of a shoulder feature at a resistance $\approx 1/20$ of the normal state resistance (R_N), by supposing the presence of two distinct, preferred cross sectional areas, one, which is 90% of the other. The success of this two cross sections model is an indication that additional fluctuation in the wire cross section is unlikely to be significant. Other indications of wire homogeneity include: 1) comparable critical current density in the two wires (Table 1), 2) all the I-V (in constant current mode) show evidence for one criti-

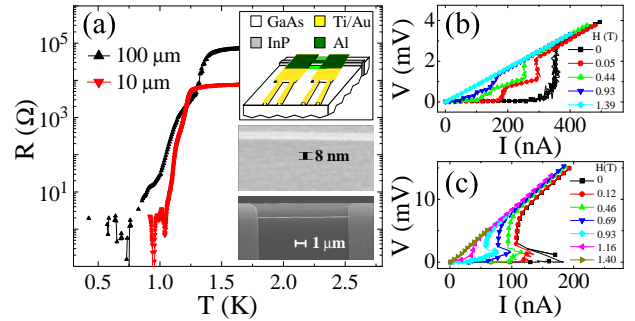


FIG. 1: (Color online) Transport properties for samples s1 and s2. (a) N-S transition. At temperatures below ≈ 1 K, samples s2 (100 μ m long, $R_N = 86k\Omega$, \blacktriangle) and s1 (10 μ m long, $R_N = 8.3k\Omega$, \blacktriangledown) became superconducting. The insets show SEM images and schematic of a typical device containing a 10 μ m long, nominally 8 nm wide Al nanowire (similar to samples s1 and s2): the Al layer does not cover entirely the Au/Ti pads which were measured in series with the superconducting wire (in panel a this series resistance has been subtracted). (b-c) Current-voltage (I-V) characteristics at $T = 0.38$ K, in different magnetic fields. In both samples s1 (b) and s2 (c), the I-V (in constant voltage mode) showed stepped structure at $T \ll T_c$. The traces are not hysteretic and at $H = 0$ T show unusual temporal noise, which was eliminated by the application of the magnetic field.

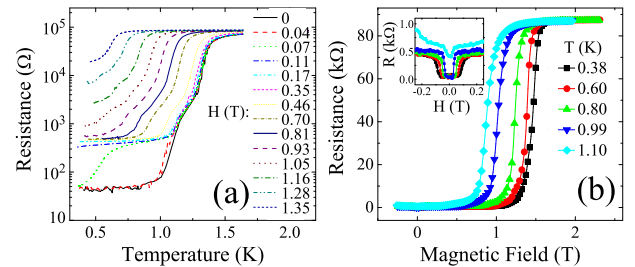


FIG. 2: (Color online) Four terminal resistance for sample s2. The resistance of sample s2 has been measured at fixed magnetic field (a) and at fixed temperature (b). (b-inset) The measured resistance increases upon reaching the critical field for the region of the pads covered by aluminum.

cal current which drives the nanowire into normal state (shown for sample s2 in Fig. 3(i)-(l)). Evidence for the 1D nature of the superconductivity can also be seen in the current-voltage traces (in constant voltage mode) shown in Fig. 1(b)-(c), where non-hysteretic characteristic voltage steps and S shaped curves [15, 18] are found down to $T/T_c \approx 0.2$. The measured four-terminal resistance for wire s2 as a function of temperature in different magnetic fields, H , is displayed in Fig. 2(a). These data, together with the I-V curves, represent the main focus of our analysis. To properly analyze the R vs. T data, all series resistances must be properly accounted for. Particular care must be taken in quantifying the contribution of the pads, a portion of which is superconducting near zero field and normal otherwise (Fig. 2(b) and inset)[19] and

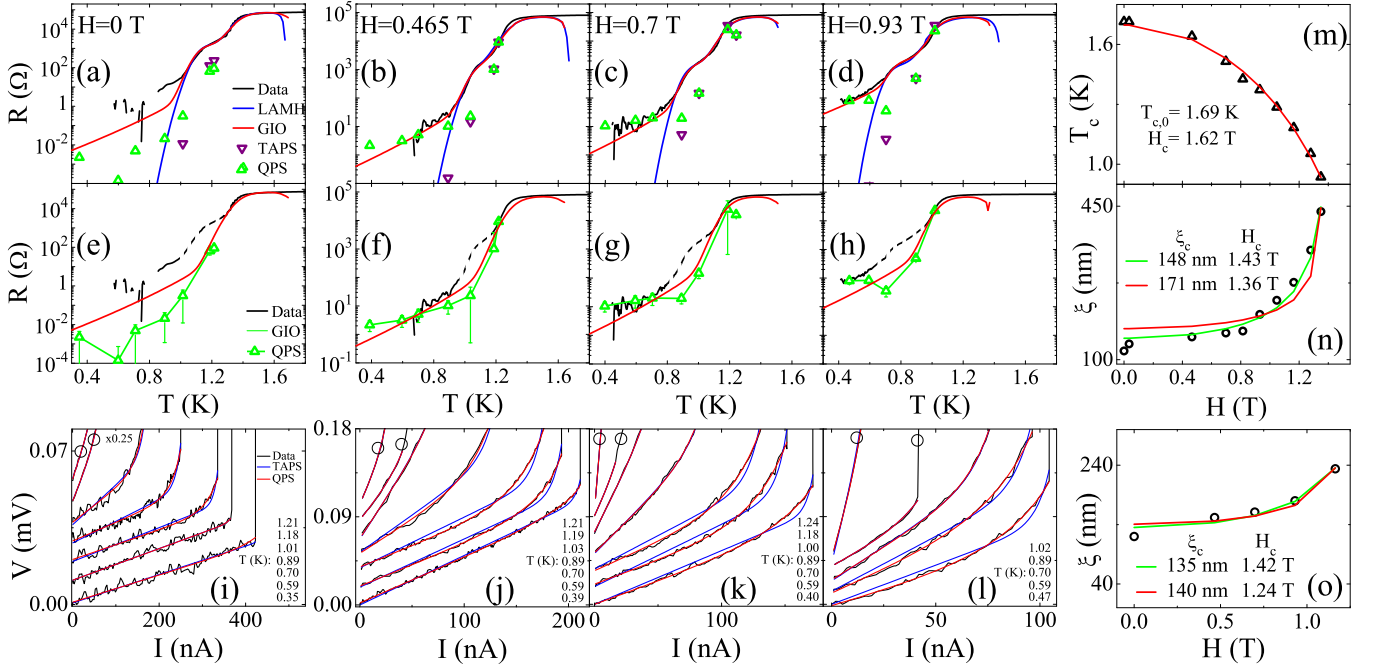


FIG. 3: (Color) N-S transition and I-V characteristics at representative values of the magnetic field. (a)-(d) Experimental data (black), after background subtraction, for sample s2 and fit to the LAMH (blue) and GIO (red) theories; the resistance due to phase slips, extracted from fit to the I-V (R_{TAPS} ∇ ; R_{QPS} Δ), are also shown. (e)-(h) Disregarding the shoulder feature (dashed in these graphs), the N-S transition at $T \lesssim T_c$ (black) and R_{QPS} (green), extracted from the I-V fits in (i)-(l) (already shown in (a)-(d)), have been refitted using the GIO model (red) with the same a_{GIO} and B_{GIO} as before. (i)-(l) Non-linear I-V characteristics (offset for clarity, \circ indicates curves multiplied by 0.25) are shown together with fits to the expressions for TAPS (blue) and TAPS+QTPS (red). These data are fit equally well by using a power law model $V = V_s + K \cdot (I/I_k)^\nu$ where $12 \gtrsim \nu \gtrsim 2$ for $0 \leq B \leq 1.1$ T [12, 13]. (m)-(n) T_{c1} (Δ), and ξ (\bullet), as deduced by the fit to the GIO theory (a)-(d), are plotted as function of H and fit to the theoretical expressions described in the text (red line). ξ is better described by $\xi = \xi_c / \sqrt{1 - (H/H_c)^2}$ (green line). (o) ξ obtained from the fits in 3(e)-(h) has been fit with the GL expression (red line) and with (green line) which better describes its behavior ($\xi_c \equiv \xi(H=0)$ is within 5% of the value in Table 1).

possible systematic error will be corrected in the last section, where the non-linear I-V behavior will be analyzed to extract the resistance contribution directly relevant to phase slip processes. Curve fitting to the extracted traces was performed following Lau et al.[14]. A superconducting wire is considered normal for $T > T_c$, while for $T \leq T_c$, it is modeled as a normal and a superconducting wire in parallel, the latter with a resistance which is the sum of the classical and quantum phase slip contributions. As stated above, we assume our wire to be composed of segments of two slightly different cross sectional areas, with a fixed ratio of 90% ($\Delta F \propto A$), and different critical temperatures. Since in Al nanowires a smaller cross section correspond to a larger T_c [20], the thinner segments, with critical temperature (resistance) T_{c1} (R_1), are responsible for 90% of the normal resistance. At zero field, the fitting parameters are $T_{c1}(H=0)$, $T_{c2}(H=0)$, $\xi(H=0)$, R_1 , a_{GIO} , and B_{GIO} , while at $H \geq 0.465$ T, only $T_{c1}(H)$, $T_{c2}(H)$, $\xi(H)$ were varied to fit our data. Fits using two different ξ_i 's were also attempted and although better results were obtained, ξ_2 (the superconducting coherence length for the wider cross sectional

region) turned out to behave in an unphysical way, tending to decrease rather than increase with increasing H. Our fits to the LAMH and GIO theories are shown in Fig. 3(a)-(e) for representative values of the magnetic field. While at zero field both theories provided reasonable fits over several decades in resistance and are nearly equivalent above ≈ 60 Ω , at higher field the GIO theory clearly better models the data beyond experimental uncertainty, particularly in the important tail region. We were able to fit our data with $a_{GIO} = 1.2$ and $B_{GIO} = 1$, which will be used throughout the analysis of the non-linear I-V (Fig. 3(e)-(l)). These values are thus in agreement with the expectation of order unity. Since both T_c and ξ depend on Δ_0 ($\Delta_0 = 1.76k_B T_c$, $\xi \propto \sqrt{\xi_0 l_e} \propto 1/\sqrt{\Delta_0}$ with ξ_0 the GL superconducting coherence length in bulk Al and l_e the electron mean free path in the nanowire) and, according to the GL theory, $\Delta = \Delta_0 \sqrt{1 - (H/H_c)^2}$, we have modeled T_c and ξ with:

$$T_{c1} = T_{c,0} \sqrt{1 - (H/H_c)^2} \quad \xi = \xi_c / \sqrt[4]{1 - (H/H_c)^2} \quad (4)$$

where $T_{c,0}$ and ξ_c are the zero field values and H_c the critical field (Fig. 3(m)-(n), red line). The critical tem-

perature of the longest segment (T_{c1}) agrees remarkably well with the theoretical expression in further support of our interpretation of a resistive transition dominated by the quantum tunneling of the order parameter's phase. A similar accord is observed for T_{c2} as well. For ξ as shown in Fig. 3(n), we can obtain a better agreement if we assumed $\xi = \xi_c / \sqrt{1 - (H/H_c)^2}$ (green line). These results, which indicate that the N-S transition of sample s2 exhibited non-classical phase slip behavior in the presence of an applied magnetic field, are supported by a detailed analysis of the non-linear I-V characteristics. Extending the analysis of Rogachev et al.[16] by including QTPS and to account for series resistances, we assumed that the total voltage drop across the superconducting nanowire is $V = V_{TAPS} + V_{QTPS} + V_S$ where $V_S = R_S I$ and R_S is a series resistance which includes the contribution of the pads and any other possible ohmic-like contributions such as proximity effect of the normal pads[21] on the superconducting wire. In this model R_{TAPS} , R_{QTPS} and R_S are fitting parameters[22] ($R_{QPS} = R_{QTPS} + R_{TAPS}$) while T_c (dependent on magnetic field which enters in the fit through τ_{GL}) and a_{GIO} have been deduced from the fit to the R vs. T data. For comparison we also fitted the experimental data with $V = V_{TAPS} + V_S$ with R_{TAPS} and R_S as fitting parameters from which we extracted the resistance due to thermal phase slips alone (R_{TAPS}). As can be seen from the fits to the I-V curves (Fig. 3(i)-(l)), classical phase slips alone reproduced the data only at the highest field and/or temperature examined. At all other fields and temperatures, the experimental data were adequately fitted only by including V_{QTPS} : the statistical (random variable) F-test, applied to the two models, supports the presence of quantum phase slips (in the form we have proposed) with a confidence above 99.99%[23]. In the EPAPS supplement[24], we will show that due to the presence of the InP ridge, even at a power ≈ 10 pW dissipated in the nanowire, the self-heating is not important for the data shown in Fig. 3(i)-(l) and Fig. 4. This is in contrast to other systems where the 1D superconducting wire is fabricated on suspended nanotube[25] and measurements taken at much lower temperature. To additionally emphasize the quantitative differences between the two models, in Fig. 4 we have reproduced representative curves from Fig. 3(j)-(l) after subtracting the series resistance, R_S , whose contribution is linear with the current. The inclusion of V_{QTPS} , is crucial to obtain quantitative agreement with the data. Additionally, as can be seen in Fig. 3(a)-(d), R_{QPS} is closer to the R vs. T data than R_{TAPS} . Deviations from the N-S curves are observed in the region of the shoulder feature, which is not included in our simple model of the I-V[26], and also at higher magnetic field (above 1 T) where the proximity effect of the normal pads might contribute more significantly to the measured four terminal resistance. We have, therefore, attempted to reproduce, using the GIO model, the superconducting transition at $T \lesssim T_c$

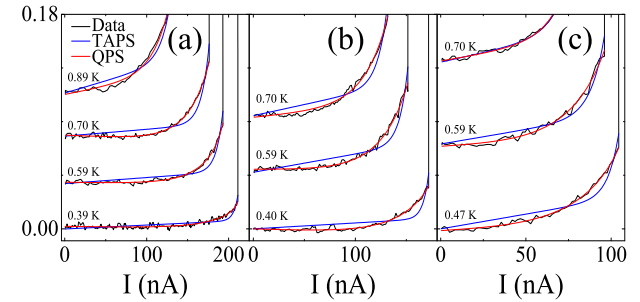


FIG. 4: (Color) Representative curves from Fig. 3(j)-(l) have been reproduced in Fig. 4(a)-(c) respectively (offset for clarity), after subtracting the series resistance, to emphasize the quantitative agreement between the QPS model and the experimental data.

and R_{QPS} obtaining satisfactory agreement as shown in Fig. 3(e)-(h). While there was no significant change for T_{c1} , at higher field ξ needed to be reduced (compared to the N-S fit) to adequately reproduce R_{QPS} . Similar to Fig. 3(n), curve fitting for the new values of ξ (Fig. 3(o)) with $\xi = \xi_c / \sqrt{1 - (H/H_c)^2}$ better reproduces the data and yielded a value $\xi_c \equiv \xi(H=0) \approx 135$ nm, within 5% of the value calculated in Table 1. As a consistency check, a similar analysis on the I-V curves of sample s1 did not produce any noticeable sign of QTPS for $H \lesssim 0.9$ T. This is sensible because, only at this higher field does the free energy barrier ($\Delta F/k_B T_c$) for sample s1 become comparable to that in sample s2 at a field $H \approx 0.465$ T, where QTPS first become important. These results establish on firm ground the importance of macroscopic quantum tunneling in the phase slip process at temperature much lower than T_c and pave the way to the study of quantum phase transitions predicted in superconducting nanowires connected to normal or superconducting reservoirs[27].

F.A. would like to thank M.E. Rizza for her support, A. Bove, J.C. Chen and P. Li for discussions. This work has been in part supported by NSF DMR-0135931 and DMR-0401648.

- [1] A. Bezryadin *et al.*, *Nature* **404**, 971 (2000).
- [2] N. A. Melosh *et al.*, *Science* **300**, 112 (2003).
- [3] D. Natelson *et al.*, *Solid-State Commun.* **115**, 269 (2000).
- [4] H. Yan *et al.*, *Science* **301**, 1882 (2003).
- [5] F. Altomare *et al.*, *Appl. Phys. Lett.* **86**, 172501 (2005).
- [6] J. S. Langer and V. Ambegaokar, *Physical Review* **164**, 498 (1967).
- [7] D. E. McCumber and B. I. Halperin, *Phys. Rev. B* **1**, 1054 (1970).
- [8] R. S. Newbower *et al.*, *Phys. Rev. B* **5**, 864 (1972).
- [9] N. Giordano, *Phys. Rev. Lett.* **61**, 2137 (1988).
- [10] D. S. Golubev and A. D. Zaikin, *Phys. Rev. B* **64**, 014504 (2001).

- [11] A. D. Zaikin *et al.*, Phys. Rev. Lett. **78**, 1552 (1997).
- [12] S. Khlebnikov, unpublished; S. Khlebnikov and L. P. Pryadko, Phys. Rev. Lett. **95**, 107007 (2005).
- [13] EPAPS Document No. (section 5) provides a brief analysis of the behavior of the exponent as function of the magnetic field.
- [14] C. N. Lau *et al.*, Phys. Rev. Lett. **87**, 217003 (2001).
- [15] M. L. Tian *et al.*, Phys. Rev. B **71**, 104521 (2005).
- [16] A. Rogachev *et al.*, Phys. Rev. Lett. **94**, 017004 (2005).
- [17] Electrical measurements were performed with a PAR 124A lockin-amplifier at 23 Hz and a current of 1.6 nA in a ^3He cryostat. Room temperature RC filters were used to protect the sample and reduce the electrical noise. Moreover, the sample lead resistances ($\approx 2\text{-}20\text{ }k\Omega$) and lead capacitances to ground ($\approx 0.5\text{ nF}$) formed natural low temperature RC filters for the Al nanowires.
- [18] D. Y. Vodolazov *et al.*, Phys. Rev. Lett. **91**, 157001 (2003).
- [19] See EPAPS Document No. (section 1) for details.
- [20] M. Savolainen *et al.*, Appl. Phy. A **79**, 1769 (2004).
- [21] G. R. Boogaard *et al.*, Phys. Rev. B **69**, 220503(R) (2004).
- [22] In order to distinguish the fitting parameter values from the theoretical ones, we refer to R_{TAPS} (R_{QTPS}) as the TAPS (QTPS) resistance extracted from the fit to the I-V, and to R_{LAMH} (R_{GIO}) as the calculated values for TAPS (QTPS).
- [23] See EPAPS Document No. (section 2) for details on the F-test.
- [24] See EPAPS Document No. (section 3) for details.
- [25] A. Johansson *et al.*, cond-mat/0505577 (2005).
- [26] See EPAPS Document No. (section 4) for details.
- [27] S. Sachdev *et al.*, Phys. Rev. Lett. **92**, 237003 (2004).

Non-linear Current-Voltage Dependence of the Superconducting Transition in 1-D

Ultranarrow Al wires

Fabio Altomare, Albert M. Chang, Michael R. Melloch, Yuguang Hong, and Charles W. Tu

1. DETAILS ON THE SUBTRACTION OF THE SERIES RESISTANCE

At $H=0$ T the resistance decreases from 86 k Ω ($\gg R_q = h/4e^2 \approx 6.45$ k Ω) to 47 ± 4 Ω and saturates below 0.75 K. This residual resistance is due to the pads and is measured in series with the wire. There are two contributions from each pad: one from an Au/Ti region (47 Ω) remaining after the final aluminum evaporation, which did not overlap the Au/Ti completely, and the other from the Al/Au/Ti region (0 Ω when superconducting, and ≈ 423 Ω when normal), observable in the inset of Fig. 2(b) as the first resistive transition near $H = 0.1$ T. This conclusion is reached after separate two terminal measurement of each pad alone, which confirmed the presence of this transition, as well as an independent four-terminal measurement on a different Al/Au/Ti trilayer sample with the pad's geometry. At 0.34 K, the total pad resistance becomes independent of H above $H \approx 0.35$ T, having attained the full normal state value of ≈ 470 Ω which, above this field, is temperature independent. To extract the wire resistance alone, we subtract this resistance of 470 Ω from the R vs. T traces when $H \geq 0.465$ T, while for $H \leq 0.03$ T we subtract 47 Ω instead, since the Al/Au/Ti superconducts below ≈ 1 K. The precise subtracted values were deduced from curve fitting.

2. F-TEST

V_{TAPS} (Eq. 1) does not depend on the magnetic field which enters in V_{QTPS} through τ_{GL} . The presence of TAPS was checked by fitting the experimental data to $V = V_{TAPS} + V_S$, where $V_S = R_S I$ (it represents the contribution due to the ohmic-like resistances in series with the superconducting wire) with R_{TAPS} and R_S as fitting parameters[1]; quantum phase slips (QPS) were fit using $V = V_{TAPS} + V_{QTPS} + V_S$ with R_{TAPS} , R_{QTPS} and R_S as fitting parameters ($R_{QPS} = R_{QTPS} + R_{TAPS}$). T_c (dependent on magnetic field) and a_{GIO} have been deduced from the fit to the R vs. T data. In order to distinguish the fitting parameter values from the theoretical ones, we refer to R_{TAPS} (R_{QTPS}) as the TAPS (QTPS) resistance extracted from the fit to the I-V, and to R_{LAMH} (R_{GIO}) as the calculated values for TAPS (QTPS). As can be seen in Fig. 4 in the main text, the inclusion of V_{QTPS} , is crucial to obtain quantitative agreement

with the data. In order to compare the two different fitting models, the F-test has been applied to the random variable $F(n, m) = [(\chi_{QPS}^2 - \chi_{TAPS}^2)/\chi_{QPS}^2]/[(df_{QPS} - df_{TAPS})/df_{QPS}]$. Here $n = df_{QPS} - df_{TAPS}$, $m = df_{QPS}$ with df the number of degree of freedom, in the model under exam, defined by $df = N - p$ and $\chi_{QPS}^2(\chi_{TAPS}^2)$ represents the chi-square obtained by fitting the experimental data to the QPS (TAPS) model: $\chi^2(a_1 \cdots a_n) = \frac{1}{df} \sum [y_i - f(x_i, a_1 \cdots a_n)]$, with y_i and x_i the experimental data and $a_1 \cdots a_n$ fitting parameters.

In this expression, N is the number of points and p the number of fitting parameter in the model. To accept the QPS model and refuse the TAPS one with a confidence level exceeding 99%, $F(n, m)$ has to exceed the criterion for an integrated probability of 99% in the $F(n, m)$ distribution with n and m degrees of freedom. In our calculations the QPS model is preferred[2] with a confidence level greater than 99.99%.

3. ESTIMATE OF SELF-HEATING

In this section of the EPAPS we will show that any heating effect that may arise from the non-negligible power level dissipated in the superconducting wire, has minimal effects in the analysis of the nonlinear I-V curves of Fig. 3 (main paper) for $I < I_C$ and can be neglected, without loss of generality, in our fitting procedure. We will also show that it is reasonable to ascribe the dominant thermal conduction to the lattice conduction of the InP ridge. After providing some preliminary details, we will show that, at a power of 15 pW dissipated through the nanowire and at a bath temperature $T_{bath} = 0.4$ K, this self-heating would increase the wire temperature (T_w) to no more than 0.48 K (a relative change in temperature $\Delta T/T \lesssim 20\%$). Additionally, this temperature rise decreases with increasing bath temperature, due to increased thermal conduction of the InP ridge on which the nanowire sits, and, under the same assumptions, at $T = 0.6$ K the relative change in temperature would be $\Delta T/T \lesssim 4\%$ and at $T = 0.7$ K $\Delta T/T \lesssim 2.3\%$: this change in temperature alone, which does not depend on the magnetic field, cannot account for the observed non-linearity in the I-V. Our situation is in direct contrast with the results presented in other works where the superconducting wire was fabricated on suspended nanotubes[3, 4] and therefore lacked a direct thermal link to the substrate aside from the wire itself, for which, the electron thermal conductivity deduced from the electrical conductivity via the Wiedemann-Franz relation, was the dominant (but inadequate) means for thermal conduction. In particular, in the work of Johannsson et al., heating seriously limits the range of viable currents at their measuring temperature (~ 10 mK, much lower than in the present work). The two systems, however, cannot be directly compared because in the suspended nanotube geometry, the only additional cooling effect, beyond the electric thermal conduction, is due

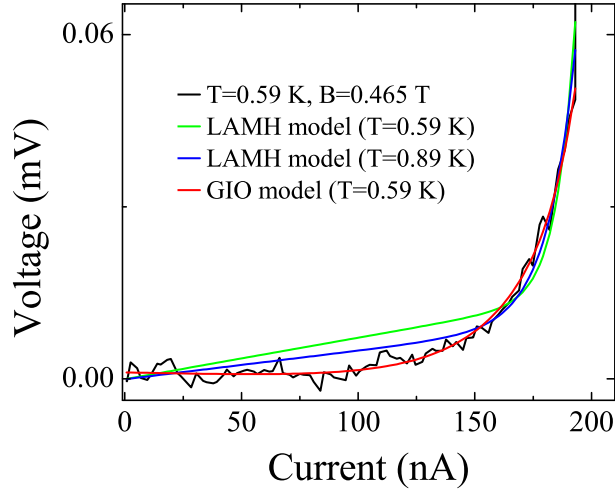


FIG. E1: (Color) Even by changing the temperature by as much as 50% the LAMH model does not properly reproduce the experimental data (here shown for $T=0.6$ K and $B=0.465$ T) as well as the GIO model. The traces are shown after subtracting the contribution due to the linear series resistance.

to the ^3He bath which is negligible because of the Kapitza boundary resistance. In our case the InP ridge, on which the wire is fabricated, readily thermalizes with the wafer; this in turn, because of its large (compared to the nanowire and the ridge) physical size ($0.5\text{ mm} \times 1.5\text{ mm} \times 2\text{ mm}$) is not affected by the Kapitza boundary resistance and can be efficiently cooled by the bath. We will demonstrate that, a) assuming a constant effective wire temperature (T_w), but higher than the bath temperature (T_{bath}), the LAMH theory still cannot properly reproduce the experimental data; b) the small increase in temperature we estimate, and the associate increase in resistance, is not nearly sufficient to explain the observed non linearity and, even by modifying our fitting procedure so as to include this temperature change into a temperature dependent coefficient, the LAMH model does not adequately describe the experimental data. On the other hand, the GIO model at all temperatures and fields examined, fits the data well.

The first point (a) is readily proven in Fig. E1 where the experimental data (for a representative trace displayed in Fig. 4 of the main paper) are fitted with the LAMH theory by changing the temperature by as much as 50%: the agreement between the LAMH model and the experimental data is still poor when compared to the GIO model.

Regarding the second point (b), in order to render the discussion more quantitative, some observations need to be noted:

- 1) The power dissipated in the wire can be deduced from Fig. 3(i)-(l) using $V \cdot I = R \cdot I^2$ after subtracting the contribution due to the pads — $50\text{ }\Omega$ at $B=0$ T and $460\text{ }\Omega$ at $B \geq 0.465$ T. Immediately before switching from the

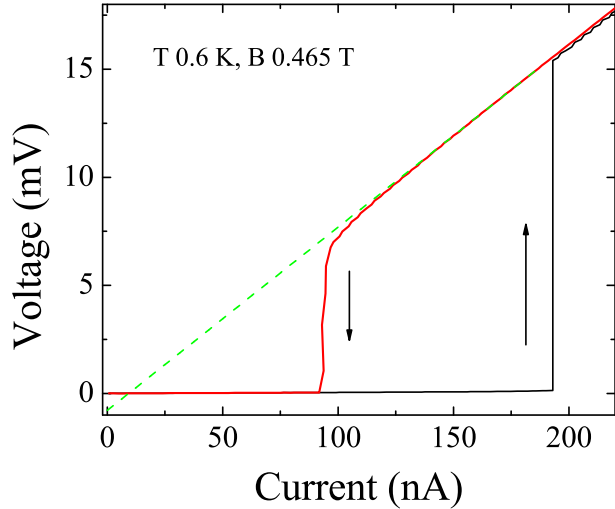


FIG. E2: (Color) I-V characteristic for the up (black) and down (red) sweep at $T=0.59$ K and $B=0.465$ T. The dashed line intersects the current axis at a finite current indicating the presence of a nonzero average supercurrent.

superconducting state to the normal state, the power dissipated in the wire is in the range $P \approx 5 - 12$ pW. To see that the electronic thermal contribution alone is not sufficient to cool the wire, as pointed out by referee A, we use a simple estimate based on the Wiedemann-Franz law and the heat diffusion equation ($\dot{Q} = A\kappa\nabla T$), with A the cross sectional area of the wire, κ the thermal conductivity and ∇T the temperature gradient, to find that, at $T=0.5$ K, it would produce an increase in temperature of several kelvin: an entirely inaccurate scenario, since the nanowire still exhibits a non-zero critical current, and therefore the effective wire temperature is smaller than the critical temperature ($T_c \sim 1.7$ K). This can be seen most dramatically in the I-V curve in the down sweep of the current (Fig. E2, red curve), where the power in the wire, immediately before switching from the normal to the superconducting state, is greater than 200 pW. If there were no additional channels, *i.e.* the InP ridge and substrate, to conduct away the heat generated by this large power, the temperature rise would be so huge ($\gtrsim 10$ K) that no transition from the normal to the superconducting state would be observed. In fact, based on the experimental data, even at these power levels, the wire temperature cannot be above the critical temperature because a nonzero average supercurrent still flows in the nanowire. This can be deduced by noticing that the extrapolation of the down sweep I-V intercepts the current axis at a finite value (a typical curve is shown in Fig. E2 for the I-V trace taken at $T=0.59$ K and $B=0.465$ T). While this does not exclude the possibility of a slight temperature rise, it clearly excludes a naive model of thermal conduction with dominant electron component, based on the Wiedemann-Franz law, which would yield a large change in temperature. Moreover, this failure implies that the above description does not adequately

model the experimental situation.

2) Thermalization of the wire in the vertical direction ($\sim 6.1 \text{ nm}$), as opposed to along the wire through the pads can readily be achieved via electronic conduction. This means that heat can easily be transferred from the top to the bottom of the nanowire across the 6.1 nm distance (the farthest and closest to the ridge, respectively), and any difference in temperature quickly equilibrated. In fact, because of the large cross sectional $—100 \mu\text{m} \times 5.25 \text{ nm}$ —surface area (versus $5.25 \text{ nm} \times 6.1 \text{ nm}$ cross section for thermal conduction along the nanowire), even for a very high power of $P \sim 300 \text{ pW}$ (which would render the wire normal) and $T=0.5 \text{ K}$, by using the heat diffusion equation combined with the Wiedemann-Franz law, we obtain $\Delta T \lesssim 1 \cdot 10^{-5} \text{ K}$. Any heat generated in the wire, therefore, will be quickly transferred to the InP ridge which (as it will be discussed later in detail) is the dominant mechanism for thermally anchoring the wire to the bath.

3) The crystal thermal conductivity (κ) of the InP ridge and the InP/GaAs substrate is *independent of the magnetic field* and $\kappa \propto C_v \lambda_{ph}$ where λ_{ph} is the phonon mean free path and $C_v \propto T^3$ is the specific heat. For the bulk InP/GaAs substrate the phonon mean free path is limited by boundary scattering while for the InP ridge is most likely cut off by the height of the ridge ($\sim 25 \text{ nm}$). Since the ridge width is only $\sim 8 \text{ nm}$ and is almost atomically flat, the reflection off the ridge walls is likely specular (note that the thermal wavelength at 1 K is $\approx 50 \text{ nm}$). Only bulk phonons, however, will be effective in transferring the heat because surface defects and adsorbates will limit the heat transferred by surface phonons.

4) One of the biggest problems in thermally anchoring a sample at the bath temperature, in low temperature measurements, is the Kapitza boundary resistance, defined as

$$R_k = A \Delta T / \dot{Q} \quad (1)$$

where A is the contact area, ΔT the difference in temperature between the bath and the sample (nanowire in our case) and \dot{Q} the heat flow. Based on values for other typical metals[5], because of the small contact area between ^3He and the aluminum nanowire, the bath cannot properly cool the nanowire. On the other hand, the crystal size ($.5 \text{ mm} \times 1.5 \text{ mm} \times 2 \text{ mm}$) is such that any thermal boundary resistance can be ignored. Additionally, given the typical lattice conductivity of good crystals (at $T=1 \text{ K}$, $\kappa \approx 0.01 - 8 \text{ W/K m}$)[6, 7] from the heat diffusion equation, at $P=10 \text{ pW}$, the increase in temperature for the crystal would be $\Delta T \lesssim 1 \cdot 10^{-4} \text{ K}$. Based on the above discussion, since the aluminum nanowire exhibits superconducting behavior, even at power of the order of 200 pW or more (finite non-zero switching current), the temperature must still be below $T_c \sim 1.7 \text{ K}$. Therefore there must be some channel

that efficiently anchors the nanowire to the bath temperature: this channel is the InP ridge, directly connected to the crystal substrate.

Below we present a quantitative analysis of the temperature rise, at the relevant power levels of $P \lesssim 15 \text{ pW}$, for the non-linear I-V curves for Fig. 3 of the manuscript. We begin by noting that the change in resistance due to the heat is not sufficient in explaining the observed non linearity.

In fact, let's assume (this will be demonstrated later) that a power of 15 pW produces a relative increase in temperature of 20% at $T=0.4 \text{ K}$, 4% at $T=0.6 \text{ K}$ and 2.3% at $T=0.7 \text{ K}$. Because of the temperature dependence of the resistance, *i. e.* increases with increasing temperature as shown in Fig. 2a of the main paper, there will be non linearity in the I-V characteristics. Any heating effect, however, will be independent of the magnetic field, so we can use the R vs. T (in the linear regime, Fig. 2a) curve at $B=1.16 \text{ T}$ as a thermometer. This has the advantage of providing, in the temperature range of interest, the biggest change in resistance as function of the change in temperature. Since the R vs. T data, at this magnetic field, stops at $T \sim 0.48 \text{ K}$, we linearly interpolated to obtain the data at the lowest temperature ($T=0.42 \text{ K}$) by using the resistance obtained by the corresponding I-V curve (at $B=1.16 \text{ T}$), in the limit of low current. Our results are shown in Fig. E3 where both the experimental data and the voltage drop across the superconducting wire calculated from the measured resistance, by taking into account the change in temperature, are displayed, after subtracting the (linear with the current) contribution due to the series resistance. As can be seen in the figure, even by increasing our estimates by an additional 10%, the experimental data cannot be reproduced.

Therefore we can conclude that the major portion of the non-linearity cannot be attributed to self-heating.

From our discussion above, it is clear that, if we assume that the wire temperature either does not change or changes within our estimate, the QPS model better describes the experimental data (see also Fig. E8). Now, the only task left is to describe the method for obtaining the previously stated upper bound estimates ($\Delta T/T = 20\%$ at $T=0.4 \text{ K}$, $\Delta T/T = 4\%$ at $T=0.6 \text{ K}$, $\Delta T/T = 2.3\%$ at $T=0.7 \text{ K}$), which will be done by using the position of the critical current jumps in the I-V curves themselves. In particular, since the self-heating will be especially important at lower temperature, we will concentrate on the curves presented in Fig. 4 of the main paper where the difference between the GIO model and the LAMH model is the most apparent. Let us consider the situation depicted in Fig. E4(a). Here we show, at the same magnetic field $B = 0.465 \text{ T}$, up (black) and down (red) sweep at a bath temperature of $T = 1.04 \text{ K}$ and $T = 0.7 \text{ K}$. As can be seen from the graph, the current at which the wire switches from the

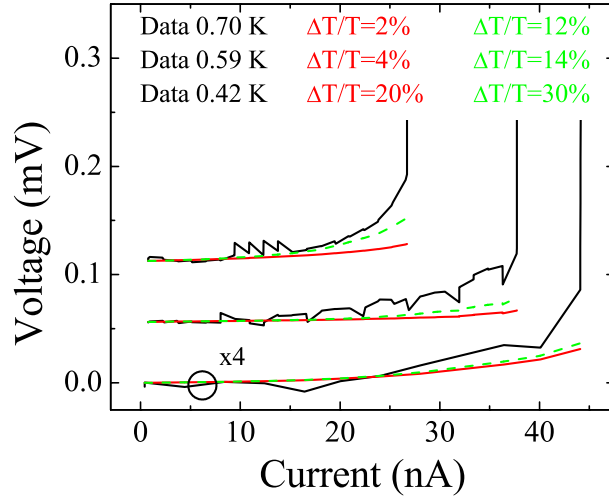


FIG. E3: (Color) Experimental I-V curves at $B=1.16$ T (black) and voltage drop across the superconducting nanowire calculated (red) up to the switching current by attributing the resistance change to the change in temperature (from bottom to top: $\Delta T/T = 20\%$ at $T=0.4$ K, $\Delta T/T = 4\%$ at $T=0.6$ K, $\Delta T/T = 2.3\%$ at $T=0.7$ K). The (linear with the current) contribution due to the series resistance has been subtracted and \circ indicates curves multiplied by 4. Even after increasing our estimate by an additional 10% (green) the agreement is still poor. Curves are offset for clarity.

normal to the superconducting state (at this current the power dissipated is $P \sim 600$ pW), for a bath temperature $T_{bath} = 0.7$ K in a down-sweep (red), is equal to the current at which, for a bath temperature $T_{bath} = 1.04$ K in a up-sweep (green), the nanowire switches from the superconducting to the normal state. Since the curves in the normal and superconducting state overlap, we can infer that, at a bath temperature $T_{bath} = 0.7$ K, the wire temperature is not more than $T_w = 1.04$ K despite a power level $P \sim 600$ pW. This is equivalent to saying that, with a power $P \sim 600$ pW dissipated in the nanowire, at a bath temperature $T_{bath} = 0.7$ K, the wire temperature raises to no more than $T_w = 1.04$ K. This identification can be made because in an up-sweep, immediately before the transition from superconducting to normal state, the power level is sufficiently low that the wire temperature is very close to the bath temperature. This power of 600 pW is estimated by multiplying the current and the voltage at the switching current in the down sweep (at $T_{bath} = 0.7$ K) after subtracting the contribution due to the pads. Wherever such a good match at different bath temperatures is not obtainable (Fig. E4(b)), we linearly interpolate between two nearby temperatures to extract the value of interest (Fig. E5). The power level is determined by the product of current and voltage at the transition from the normal to the superconducting state and, as exemplified in Fig. E5, at a bath temperature $T_{bath} = 0.39$ K, the wire temperature is $T_w = 1.01$ K at a power level $P \sim 644$ pW (the power level can

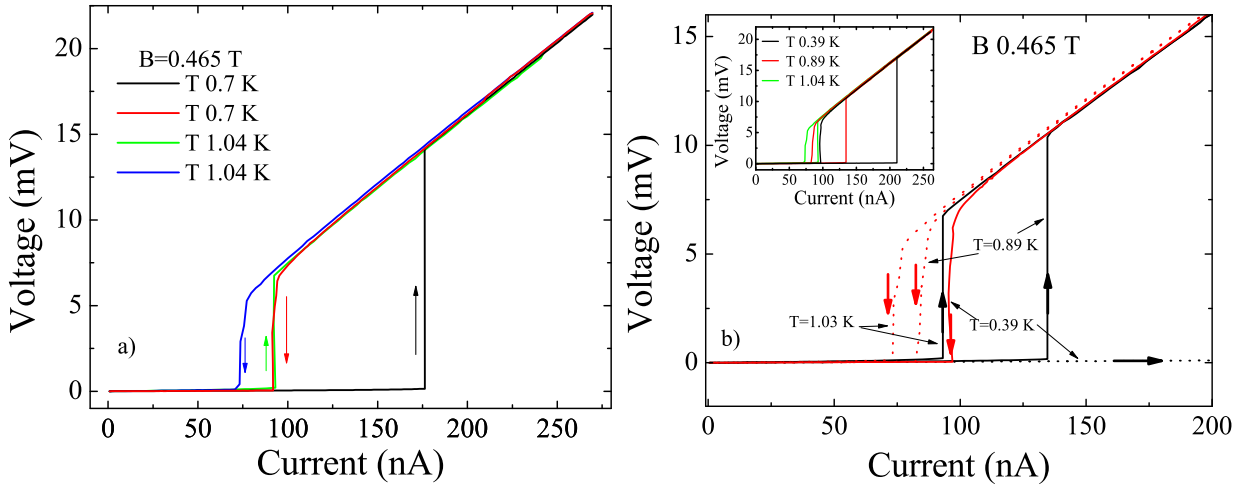


FIG. E4: (Color) $B = 0.465$ T: (a) the down sweep at $T = 0.7$ K has the same switching current as the up sweep at $T = 1.04$ K: we conclude that at $T_{bath} = 0.7$ K, a power level is $P \sim 600$ pW raises the wire temperature up to $T_w = 1.04$ K. (b) At $T = 0.39$ K, the down switching current is in between the up switching current at $T = 1.04$ K and $T = 0.89$ K. Linearly interpolating (see also Fig. E5) between these two values, we obtain that at $T_{bath} \sim 0.39$ K, a power level $P \sim 644$ pW increases the wire temperature to $T_w = 1.01$ K. The dotted curves refer to up and down sweep not relevant to this discussion. Inset: the full range of the I-V curves for the three different temperatures is shown.

be calculated from Fig. E4(b) after subtracting the pad contribution). By following this procedure for all our datasets (representative I-V are shown in Fig. E6), we obtain, for every T_{bath} of interest ($T=0.4$ K, 0.6 K and 0.7 K), the corresponding T_w as a function of the power dissipated in the nanowire. This allows us to estimate, for the lattice temperatures mentioned above, the temperature rise due to the dissipated power: in particular we will be interested in the change in temperature at the power levels at which the wire switches from the superconducting to the normal state ($\lesssim 15$ pW).

Our results are displayed in Fig. E7 (a)–(c) where the scatter in the datapoints at a given magnetic field reflects the uncertainty in the exact determination of the switching current. In order to analyze these data, we model the InP ridge thermal conductivity as a 1-dimensional problem with $P = \dot{Q} = \kappa A \nabla T$. By integrating the heat diffusion equation along the ridge height direction and taking into account the the temperature dependence (T^3) of the crystal thermal conductivity, in a scenario where $\lambda_{ph} \sim const$, the expected behavior of T_w is $T_w = \sqrt[4]{P/C + T_{bath}^4}$ with C an appropriate constant that depends on the crystal and on the ridge geometry. Note that at zero power dissipated through the nanowire (and therefore zero current flowing), the aluminum nanowire must be in thermal equilibrium with the bath.

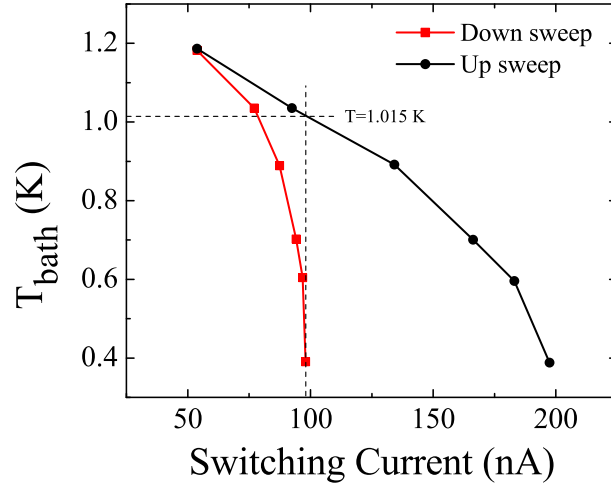


FIG. E5: At a field $B=0.465$ T, the bath temperature has been recorded as function of the up (black) and down (red) switching current. If we were to perform a measurement at $T=1.01$ K, the up switching current would be the same as the down switching current at $T=0.39$ K at a power given by the product $V \cdot I$ immediately before the transition from normal to superconducting state. By repeating the same procedure for the other fields of interest ($B=0, 0.7, 0.93$ T), we obtain the datapoints in Fig. E7 after allowing for some uncertainty in the value of the down switching current.

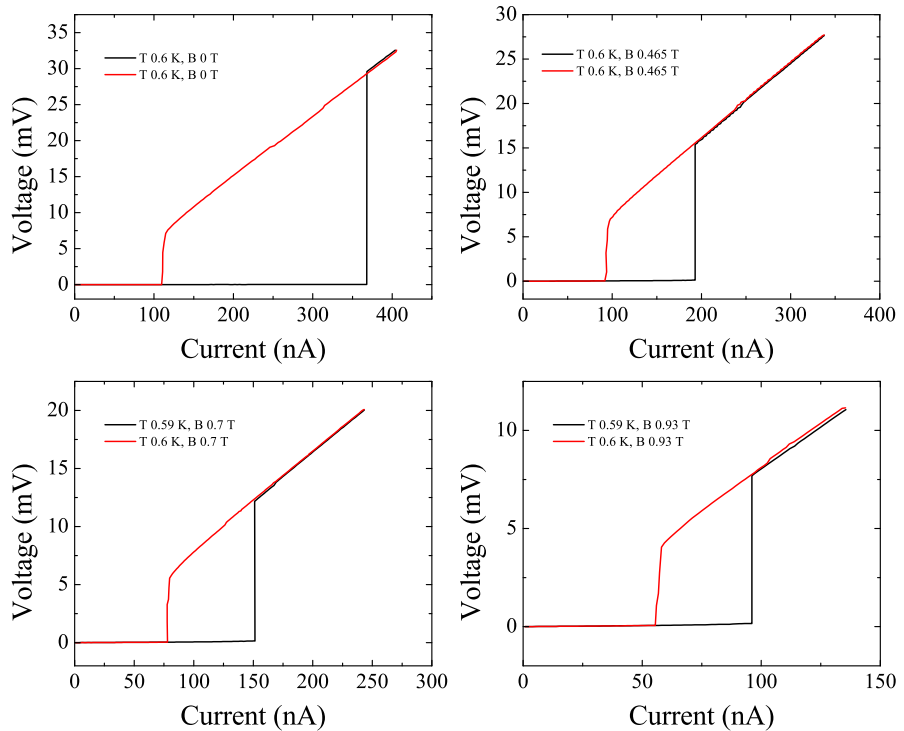


FIG. E6: (Color) Typical I-V characteristics up (black) and down (red) sweep at $T \approx 0.6$ K at different magnetic field.

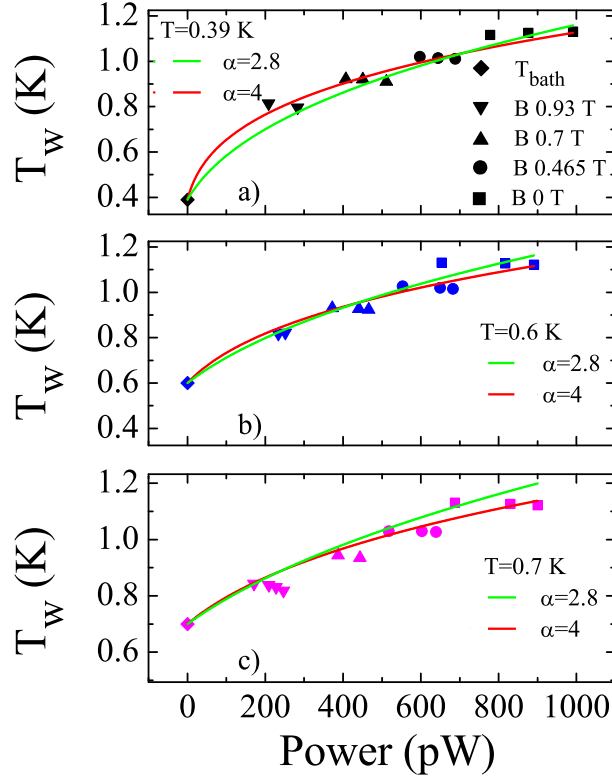


FIG. E7: (Color) Temperature reached by the superconducting nanowire at different power level and fit with the functional form discussed in the text for (a) $T_{bath} = 0.4$ K, (b) $T_{bath} = 0.6$ K, (c) $T_{bath} = 0.7$ K: the scatter in the datapoints is due to the uncertainty in estimating the value of the current at which the nanowire switches from the normal to the superconducting state. Different symbol shape indicates datapoints obtained at different fields.

From the fit to this functional form, displayed in Fig. E7, we find that, for $P=15$ pW, $\Delta T/T = 20\%$ at $T=0.4$ K, $\Delta T/T = 4\%$ at $T=0.6$ K and $\Delta T/T = 2.3\%$ at $T=0.7$ K.

It must be noted that these values are an upper bound because we have neglected the temperature dependence of the phonon mean free path (which may behave like $\lambda_{ph} \propto 1/T$ [6]): the thermal conductivity, therefore, might have a weaker dependence on the temperature. By assuming $T_w = \sqrt[3]{P/C + T_{bath}^\alpha}$, with α a fitting parameter, we obtain $\alpha = 2.8$ in good agreement with our expectations ($\alpha \simeq 3$), which would further reduce our upper bound estimate for $\Delta T/T$. By introducing this change in temperature in the coefficient R_{LAMH} and R_{GIO} employing the theoretical functional dependence, we have fit the representative curves in Fig. 4 of the main paper (Fig. E8). As can be seen, the experimental data can be adequately fit only by introducing the QPS term. These fits are nearly as good as those shown in Fig. 4 in the main paper at $T_w = T_{bath}$.

Even with the caveat that the F-test cannot distinguish any systematic errors, we want to point out that on

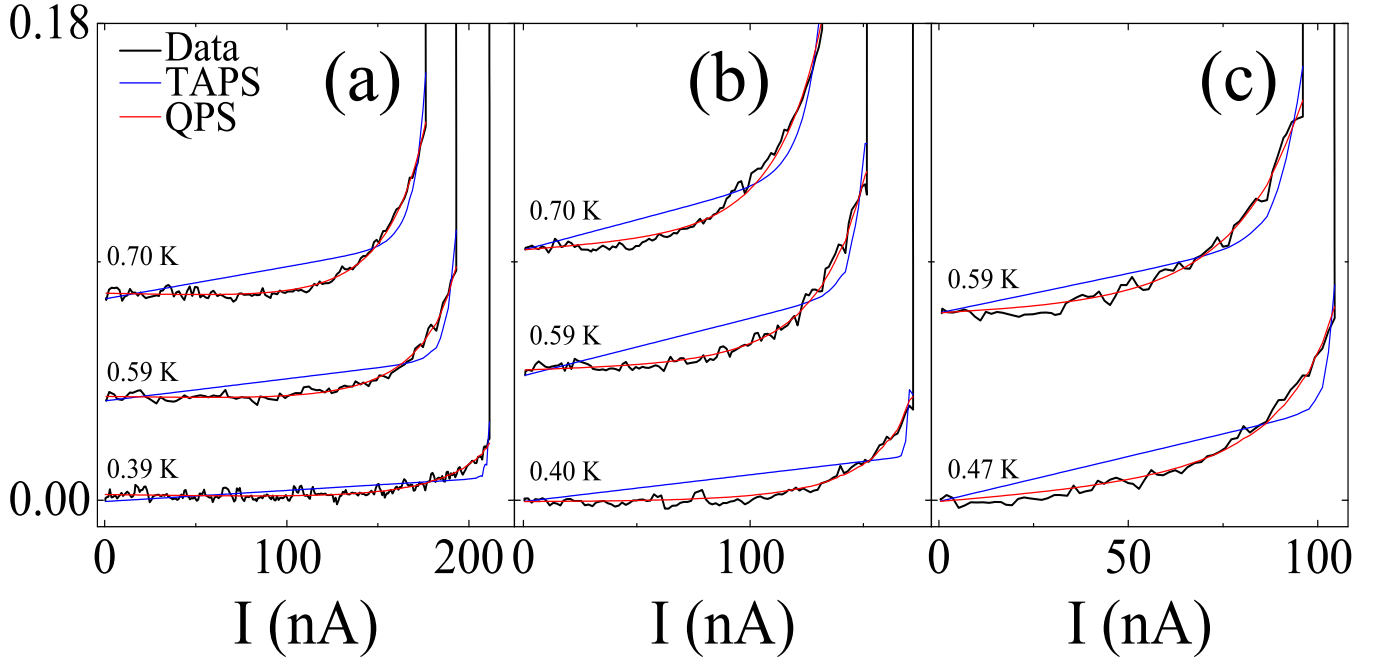


FIG. E8: (Color) The curves displayed in Fig. 4 (main paper) have been fit after including the theoretical temperature dependence in the fitting parameters R_{LAMH} and R_{GIO} . As before, only the GIO model adequately fit the experimental data at all fields and temperatures. (The linear contribution due to the series resistance has been subtracted and the curves have been offset for clarity).

the datasets in exam in Fig. E8, it supports the GIO model with a confidence level much higher than 99.99%. As an additional *independent check* on these temperature rise estimates, we would like to point out that, since the temperature increase is due solely to the power dissipated in the nanowire and should not be dependent on the applied magnetic field, we could use the non-linear I-V data at $B=1.16$ T to calculate a resistance and power level at each I and then use the R vs. T curve to convert it to an effective rough upper bound temperature *assuming that any increase in resistance comes entirely from the temperature rise alone*. By doing so we would obtain, for a power $P=15$ pW, $\Delta T/T = 31\%, 17\%, 17\% K$ at $T=0.4, 0.6, 0.7$ K, respectively. By taking into account this change in temperature, bigger than the more stringent estimate provided above, the LAMH theory would still not reproduce the data in Fig. 4 (main manuscript).

In lieu of the evidence provided, both theoretical and experimental, we can conclude that, while we cannot rule out a slight temperature increase at the power level under consideration, this change is inconsequential with respect to the main results of letter (and can be neglected): i.e. we are observing a non linearity in the I-V characteristics, which cannot be explained by the LAMH theory and is, instead, compatible with the phenomenological model of QPS.

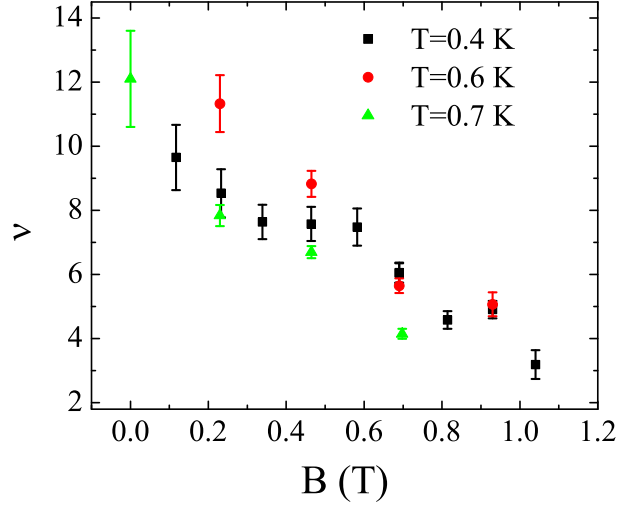


FIG. E9: The exponent ν , extracted from the fit of the I-V curves to the power law expression, has been plotted as function of the magnetic field. Different symbols correspond to I-V curves at different temperatures.

4. FIT TO THE R VS. T DATA

Due to its lower critical temperature, we interpreted the shoulder feature to arise from segments of a wider cross section; therefore, their critical current would be higher than the one of the thinner (and more resistive) segments and it would not be observable in the I-V. The same reasoning holds if, instead, the shoulder were due to some distribution in the wire width or to inhomogeneities. This follows from the dependence of the critical temperature from the cross section of SC Al nanowires (which is larger for a smaller cross section), and the absence of any stepped structure for current smaller than the critical current (at all T and H examined).

5. POWER LAW

The I-V data have been also checked against the power law dependence[8] suggested in the text:

$$V = V_s + K \cdot (I/I_k)^\nu \quad (2)$$

where $V_s = R_S I$ is due to the series resistance (R_S), K and I_k appropriate coefficients. We will not report the fit to the I-V curves since they are indistinguishable from our best fit with the GIO model; the behavior of the exponent ν as function of the magnetic field, for I-V taken at different temperatures, is shown in Fig. E9 and is consistent with naive estimates based on the theoretical model.

By following the same method described in the main letter and replacing R_{GIO} with $R_{KL} = K_1 T^{\nu-1}$ we have also

successfully fit the R vs. T data. We will not discuss those fits in detail because while the theory[8, 9] suggests that the exponent ν in the R vs. T data and in the I-V curves is the same at a given magnetic field, it provides a numerical estimate for K_1 in some very special limit. We have therefore used K_1 as a fitting parameter but by doing so, in contrast to what happens with the GIO model, the fitting function is over-parametrized.

- [1] For TAPS, we additionally imposed $V(I = 0^+) \geq 0$: marginally lower χ^2 could be obtained without this condition but this would have produced the unphysical results $V(I = 0^+) < 0$.
- [2] The F-test has been calculated using the (lower) value obtained relaxing the constraint $V(I = 0+) \geq 0$.
- [3] A. Rogachev, A. T. Bollinger, and A. Bezryadin, Phys. Rev. Lett. **94**, 017004 (2005).
- [4] A. Johansson, G. Sambandamurthy, N. Jacobson, D. Shahar, and R. Tenne, cond-mat/0505577 (2005).
- [5] G. L. Pollack, Rev. Mod. Phys. **41**, 48 (1969).
- [6] V. A. Osipov and S. E. Krasavin, Journal of Physics: Condensed Matter **10**, L639 (1998).
- [7] R. C. Zeller and R. O. Pohl, Phys. Rev. B **4**, 2029 (1971).
- [8] S. Khlebnikov, unpublished.
- [9] S. Khlebnikov and L. P. Pryadko, Phys. Rev. Lett. **95**, 107007 (2005).